Compressed Air Energy Storage System Modeling for Power System Studies

Ivan Calero, *Student Member, IEEE,* Claudio A. Cañizares, *Fellow, IEEE,* and Kankar Bhattacharya, *Fellow, IEEE*

***Abstract*—In this paper, a detailed mathematical model of the diabatic Compressed Air Energy Storage (CAES) system and a simplified version are proposed, considering independent generators/motors as interfaces with the grid. The models can be used for power system steady-state and dynamic analyses. The models include those of the compressor, synchronous motor, cavern, turbine, synchronous generator, and associated controls. The configuration and parameters of the proposed models are based on the existing bulk CAES facilities of Huntorf, Germany. The models and performance of the CAES system are first evaluated with step responses, and then examined when providing frequency regulation in a test power system with high penetration of wind generation, comparing them with existing models of CAES systems. The simulation results confirm that the dynamic responses of the detailed and simplified CAES models are similar, and demonstrate that the simultaneous charging and discharging can significantly contribute to reduce the frequency deviation of the system from the variability of the wind farm power.**

***Index Terms*—CAES, dynamic modeling, energy storage, frequency regulation, frequency stability.**

NOMENCLATURE

Indices

b	Inlet to the high pressure burner
c	Compressor
d	Inlet to the expander
e	Electrical
g	Generator
HP	High pressure
hx	Heat exchanger
i	Isentropic
in	Input
j	Index of compression stages
k	Index of expansion stages $k = \{LP, HP\}$
LP	Low pressure
m	Mechanical
max	Maximum
min	Minimum
mot	Motor
o	Nominal value
out	Output
r	Recuperator
ref	Reference or initial value
s	Storage (Cavern)
t	Turbine
x	Exhaust
w	Wind

Parameters

ϵ	Effectiveness
η	Efficiency [p.u.]
γ	Heat capacity ratio c_p/c_v
π	Pressure ratio
τ	Time constant [s]
τ_3	Radiation shield time constant [s]
τ_4	Thermocouple time constant [s]
τ_{AV}	Air valve positioner time constant [s]
τ_{CD}	Compressor volumetric time constant [s]
τ_{IGV}	IGV system time constant [s]
τ_{CP}	Compressor power transducer time constant [s]
τ_{Dr}	Compressor transient droop time constant [s]
τ_{TP}	Turbine power transducer time constant [s]
τ_R	Recuperator time constant [s]
τ_S	Fuel valve positioner time constant [s]
τ_{SF}	Fuel system time constant [s]
τ_{TD}	Turbine discharge delay [s]
Φ	Compressor's stage power constant [p.u./K]
a_1	Compressor's map coefficient
a_2	Compressor's map coefficient
c_1	No-load fuel compensation constant [p.u.]
c_2	No-load fuel consumption constant [p.u.]
c_p	Specific heat capacity at constant pressure [kJ/kg.K]
c_v	Specific heat capacity at constant volume [kJ/kg.K]
D	Damping power coefficient [p.u.]
l	IGV system limit [p.u.]
F	Fuel control limit [p.u.]
g	Air valve limit [p.u.]
H	Inertia constant [s]
K_4	Radiation shield gain
K_5	Radiation shield gain
K_{AGC}	AGC gain
K_{c_d}	Compressor's governor derivative gain
K_{c_i}	Compressor's governor integral gain
K_{c_p}	Compressor's governor proportional gain
K_{droop}	Compressor transient droop [p.u.]
K_{t_i}	Turbine's governor integral gain
K_{t_p}	Turbine's governor proportional gain
K_{T_i}	Temperature controller integral gain
K_{T_p}	Temperature controller proportional gain

This work has been funded by the Ontario Centres of Excellence (OCE), the Natural Sciences and Engineering Research Council of Canada (NSERC) Grant, and the NSERC Energy Storage Technology (NEST) Network.

The authors are with the Department of Electrical and Computer Engineering, University of Waterloo, Waterloo, ON, N2L 3G1, Canada (e-mail: icalero@uwaterloo.ca; ccanizar@uwaterloo.ca; kankar@uwaterloo.ca).

N	Frequency of filter differentiator [rad/s]
R	Regulation characteristic [p.u.]
R	Gas constant [J/kg.K]
$T_{hx_{in}}$	Inter/aftercooler cold-side input temperature [K]
T_s	Cavern temperature [K]
u	Turbine output power limit [p.u.]
V_s	Cavern volume [m^3]
v_w	Wind speed [m/s]

Variables

Γ	Compressor's stage temperature gain
$\dot{m}$	Mass of air flow rate [kg/s]
$\dot{m}_f$	Mass of fuel flow rate [kg/s]
m	Mass [kg]
P	Active Power [MW]
p	pressure [bar]
Q	Reactive Power [MVAr]
q	Heat transfer [J]
$\dot{q}$	Heat transfer rate [W]
H	Enthalpy [J]
h	Specific enthalpy [J/kg]
T	Temperature [K]
T'	Measured temperature [K]
v	Dynamic state variable [p.u.]
W	Work [J]
ω_r	Rotor speed [rad/s]
Δ	Variation
$\dot{}$	Rate of change
$\bar{}$	Per unit

I. Introduction

In the effective integration of renewable generation, energy storage systems (ESS) play a key role by providing flexibility to manage the intrinsic intermittency of energy sources such as wind and solar. In this context, only pumped-storage hydro and Compressed Air Energy Storage (CAES) are economically and technically feasible alternatives for grid scale applications [1], with CAES being less restrictive in terms of its location, especially in North America with its abundant geological formations suitable to host underground caverns for air storage [2], as in the case of the province of Ontario in Canada [3], in which the research presented here is focused.

Although CAES is a relatively old energy storage technology, very few projects have been built worldwide. Indeed, only two bulk CAES facilities are currently operating: the 290 MW Huntorf CAES plant in Germany, and the 110 MW McIntosh facility in Alabama, USA [2], [4]–[6]. This has resulted in limited data, research, and thus lack of appropriate models, especially of CAES connected to the grid. Models are particularly relevant to system operators, grid planners, utilities, and new investors to understand the grid effects of CAES systems, and their potential to provide services other than arbitrage. To this effect, this paper addresses the issue of lack of adequate models by developing a comprehensive mathematical model of the system that can be used to perform steady-state and dynamic power system studies of CAES connected to the grid.

Most of the current research on CAES system modeling has concentrated on: describing the processes from a thermodynamic perspective to evaluate internal variables such as temperatures and pressures, and performance parameters such as efficiency, for steady-state conditions [7]; simplified dynamic modeling [8], where heat exchanger delays and rotating masses are the main sources of dynamics; and studying long-term cavern dynamics (temperature, pressure, mass) [9]. In all these studies, the plant controllers, electrical machinery, and other components such as valves, actuators, or measurement systems have not been considered.

Some works have proposed models of bulk CAES systems connected to electrical grids, involving the exchange of active and reactive power. Even though CAES has the charging and discharging stages physically decoupled, most of the papers are based on a single generator/motor interfacing with the grid, which limits the full potential of CAES. For example, the use of an induction machine as generator/motor in CAES has been proposed in some papers, including [10] and [11], where the CAES system model comprises a gas turbine (GT) and a reciprocating compressor; however, the dynamics exclusively represent the gas-system controller of the GT. In [12], while a detailed model of the induction machine is presented, the compressor is modeled by algebraic equations only, and the turbine model is not considered. In [13], a CAES system is modeled for dynamic reactive power compensation while operating in idling mode, showing better performance, in some cases, than a Static Var Compensator (SVC). In [14], a CAES system is used to provide reactive power support in both idling and charging mode; however, in the last two papers, only the CAES generator component is modeled, ignoring the thermodynamics of the compressor, and no insights on the compressor-motor system or controls are provided. In [15], the authors propose two CAES system configurations based on separate motor and generator for frequency regulation; the first uses compressed air to enhance the combustion of a GT, while the second uses the remanent heat of a GT to heat up the CAES system airflow before it is expanded, thus modeling an adiabatic CAES. However, important dynamics are not considered in the model, such as, intercoolers, aftercooler, recuperator, and temperature control system for the expander; it is also assumed that the remanent heat of the GT is sufficient to make the CAES system expander operate properly.

Models based on power-electronic converter interfaces are proposed in [16] and [17], wherein, the CAES system input/output power is rectified by converters connected to a dc-link, with a grid connection through a voltage source converter (VSC). However, such a configuration is not practical for bulk applications, as the converters must be appropriately sized to handle the large discharging/charging power. The modeling of small CAES systems based on a VSC interface are also studied in [18] and [19].

Even though some of the previously discussed papers introduce models to address a particular CAES system application, none of them propose a unified model that includes all its components, i.e., cavern, turbine, compressor, generator, mo-

tor, and controls. Furthermore, these works do not model the CAES system using separate synchronous machines properly interfaced with the mechanical subsystems.

Therefore, the present paper addresses these shortcomings by proposing a comprehensive mathematical model of diabatic CAES systems considering two independent synchronous machines (generator and motor), which would allow to explore the full potential of CAES systems for electrical grids. A detailed mathematical model of a diabatic CAES system and a simplified version are proposed based on the existing Huntorf CAES system in Germany [6], and a commercially available CAES system [20]. The models presented here are first evaluated with step responses and then demonstrated on a power system with high penetration of wind generation, to illustrate the frequency regulation capabilities of CAES systems, comparing them with the models proposed in [15] and [16].

The rest of the paper is organized as follows: Section II describes the main components of a CAES system. In Section III, the proposed detailed and simplified models are described. In Section IV, the results of simulations of the proposed and existing models for step changes and frequency regulation studies in a power system with high penetration of wind generation are presented and discussed. The main conclusions, contributions, and scope for future work are highlighted in Section V.

II. Overview of Diabatic CAES Systems

In charging mode, a CAES compressor driven by an electrical motor pressurizes the air at ambient conditions, which is carried through pipes, cooled down in intercoolers and an aftercooler, and stored in the cavern [2]. As the air is injected, the internal pressure of the reservoir and its potential energy increases. In diabatic CAES systems, in discharging mode, the stored air is preheated in the recuperator, and is then combined with gas in the burner before being expanded; on the other hand, in adiabatic CAES systems, no gas is used, and the air is heated from a heat storage subsystem. The synchronous generator's rotor is moved by the expander to produce electricity. In idling mode [21], the CAES system is neither charging nor discharging. Fig. 1 depicts the following main components and interrelations of the underground diabatic CAES facility, based on [5] and [6].

- *Motor/Generator*: A single synchronous or induction generator/motor can be used in a CAES system. In this paper, however, the CAES system is modeled using two synchronous machines, operated and controlled independently, as in [20].
- *Compressor*: The compression train comprises a low-pressure axial compressor and a high-pressure multi-stage centrifugal compressor, to achieve the desired range of operating pressures in the cavern. A regulating valve is installed after the compression to throttle the compression pressure down to actual cavern pressure. Intercoolers and an aftercooler are designed to reduce the inlet temperature at the different compression stages and the air to cavern, to approximate isothermal compression and thus reduce the power required from the motor [22], reducing losses and thermal stress on the cavern. In Huntorf, three intercoolers and one aftercooler are used, and the same has been modeled here.
- *Turbine*: In diabatic CAES systems, the turbine has two main components: the combustion chamber (or burner) and the expander. The air from the cavern is preheated in the recuperator using the remanent heat of the air leaving the low-pressure exhaust in the expander, to increase efficiency [23]. It is then combined with fuel and burned in the high-pressure combustion chamber to achieve the desired inlet temperature to the high-pressure expander. After, the air is reheated in a low-pressure burner and expanded in the low-pressure expander; the reheating increases the efficiency of the expansion cycle, as the expansion work is proportional to the inlet temperature in a turbine. The turbine can operate in two modes: constant input pressure and variable input pressure [7]. In the former, the air is throttled so that the burner inlet pressure remains constant regardless of the cavern pressure, while in the latter, the burner inlet pressure is the cavern pressure.
- *Cavern*: Salt caverns are among the most convenient geological formations used as reservoirs for underground CAES, because of their relatively low overall cost [4], and leak-proof characteristics [24]. The capacity of energy storage depends on the size of the cavern, which is independent of the size of the turbo machinery. Consequently, the energy-to-power ratio of a CAES system is more flexible than other storage technologies.
- *Control System*: The air mass flow in the expansion stage is controlled to realize the desired output power, while the inlet temperature in the expanders (low and high pressure) are kept constant by controlling the fuel in the burners (two control loops). The compression air flow rate is regulated by moving the compressor's variable inlet guide vanes (IGVs), to control power. Consumption of the motor within a load range of 65 to 110% of the rated power [20], which may vary depending on the manufacturer.

III. CAES System Modeling

In this section, a comprehensive model of a CAES system suitable for power system studies considering two independent synchronous machines (motor and generator) is proposed, based on [6] and [20]. First, a detailed CAES model which includes all the components depicted in Fig. 1 is presented; then, a simplified model is proposed, which would facilitate its implementation in common power system packages for dynamic simulations, without significantly compromising its accuracy. Most of the variables defined in the Nomenclature section are expressed in per-unit; therefore, if the actual quantities are required, the per-unit values are multiplied by their corresponding bases. The proposed models are based on the following general assumptions [25]:

- The proportion of gas to air in the expander is very small, i.e., $\dot{m}_t + \dot{m}_f \approx \dot{m}_t$.

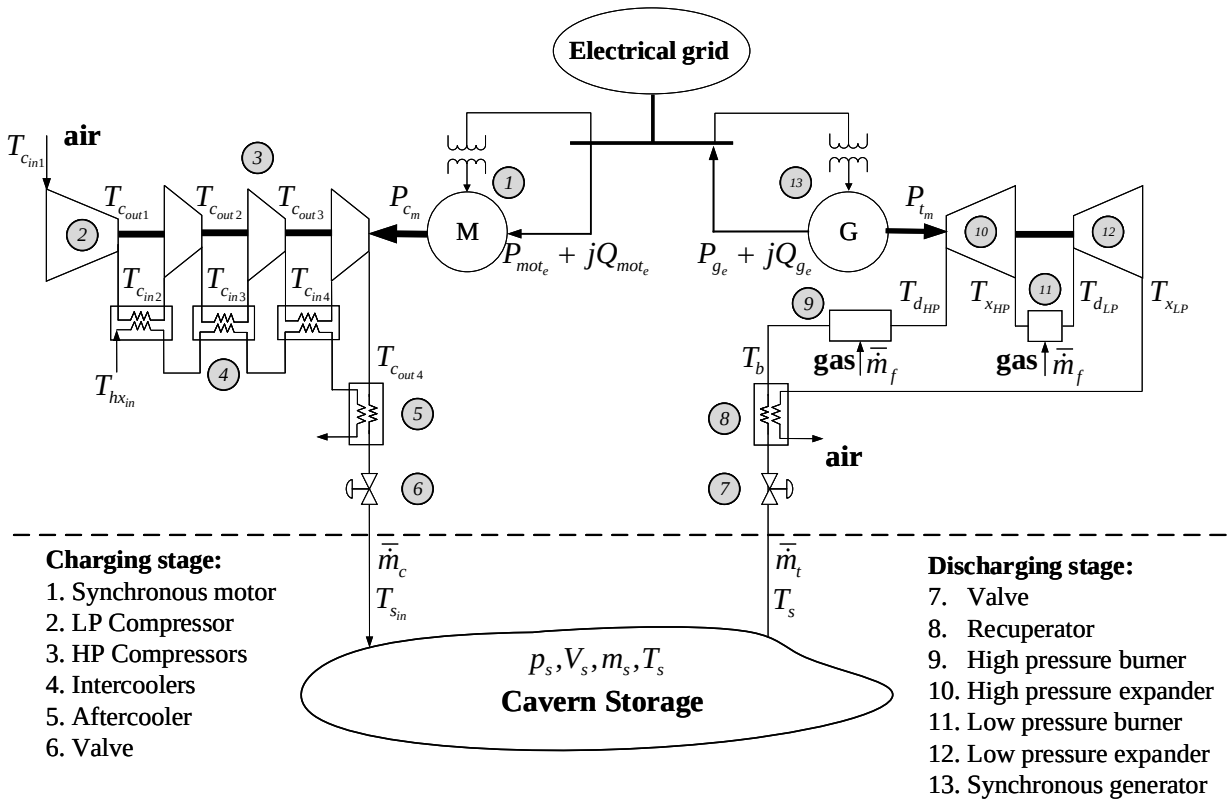

Fig. 1. Configuration of a diabatic, two-machine CAES system based on [6]. All variables are defined in the Nomenclature.

- The air behaves as an ideal gas, i.e., $\Delta h = c_p \Delta T$ for expansion and compression.
- The turbine, compressor, recuperator, intercoolers and aftercooler, and cavern are represented by steady-flow processes, i.e., the fluid flows steadily through the control volume.
- Changes in kinetic and potential energy in the processes are negligible, i.e., $q - W = \Delta \mathrm{H}$.

The detailed model is described in the following two subsections III-A and III-B, and the simplified model in Subsection III-C. The cavern model is common for both models and is presented in Subsection III-D.

A. Discharging Mode

The components involved in the discharging mode are the recuperator, combustion chambers, expanders, and synchronous generator which are described next.

1) Recuperator: The recuperator is modeled as a counter-flow heat exchanger. Its hot side is fed by the exhaust gases at temperature of the low-pressure turbine $T_{x_{LP}}$, while the air coming from the cavern enters the cold side at temperature T_s, reaching T_b at its outlet. Given that the outlet temperature of the recuperator is unknown, the heat exchanging process can be described by its effectiveness ϵ_r, defined as the ratio of the actual regenerated heat transfer rate over the maximum possible heat transfer rate as follows [26]:

$$\epsilon_r = \frac{\dot{q}}{\dot{q}_{max}} = \frac{h_b - h_s}{h_{x_{LP}} - h_s} \tag{1}$$

In this case, the maximum possible heat rate exchange ratio occurs between the inlet of the hot side and inlet of the cold side of the recuperator. It is assumed that the turbine airflow passes through both sides of the heat exchanger at the same time, i.e., input flow at hot and cold sides are the same.

From (1), acknowledging that T_b does not change instantly as heat transfer is a dynamic process, which could be approximated by a first order system [27], the input temperature of the air to the high-pressure burner $\overline{T}_b$ can be calculated as follows:

$$\overline{T}_b = \frac{T_s}{T_{b_o}} + v_r \tag{2}$$

$$\dot{v_r} = \frac{1}{\tau_R}\left[\epsilon_r\left(\frac{\overline{T}_{x_{LP}} T_{x_{LPo}} - T_s}{T_{b_o}}\right) - v_r\right] \tag{3}$$

where v_r represents the heat dynamics added by the recuperator; T_{b_o} can be found by solving (2) and (3) for steady-state conditions, and $\overline{T}_b = 1$ and $\overline{T}_{x_{LP}} = 1$.

2) Combustion Chambers or Burners: The combustion in the burners is produced by a mixture of fuel (gas) and air. In the high-pressure and low-pressure burners, the inlet temperature to their respective expanders $T_{d_{HP}}$ and $T_{d_{LP}}$ rises as the amount of fuel injected into the burners increases (mass flow rate of fuel $\dot{m}_f$), and cools down as $\dot{m}_t$ increases. In this paper, it is assumed that the fuel flow in the two burners are controlled by the same controller; hence, these vary proportionally, i.e., $\overline{\dot{m}}_{f_{HP}} = \overline{\dot{m}}_{f_{LP}} = \overline{\dot{m}}_f$. From the energy balance of the combustion chamber, and assuming isobaric

heat addition, the inlet temperature of the high-pressure and low-pressure expanders, in p.u. of their nominal values, can be obtained as follows [28]:

$$\overline{T}_{d_{HP}} = \overline{T}_b \left(\frac{T_{b_o}}{T_{d_{HPo}}} \right) + \frac{T_{d_{HPo}} - T_{b_o}}{T_{d_{HPo}}} \left(\frac{\overline{\dot{m}}_f}{\overline{\dot{m}}_t} \right) \tag{4}$$

$$\overline{T}_{d_{LP}} = \overline{T}_{x_{HP}} \left(\frac{T_{x_{HPo}}}{T_{d_{LPo}}} \right) + \frac{T_{d_{LPo}} - T_{x_{HPo}}}{T_{d_{LPo}}} \left(\frac{\overline{\dot{m}}_f}{\overline{\dot{m}}_t} \right) \tag{5}$$

where the inlet temperature of the air at the high-pressure burner is T_b, while the inlet temperature at the low-pressure burner is equal to the exhaust temperature of the high-pressure turbine $T_{x_{HP}}$.

3) Expander: For an isentropic air expansion at each stage, the corresponding isentropic exhaust temperatures $T_{x_{ik}}$ becomes a function of the turbine's stage pressure ratio π_{t_k} and inlet temperature as follows [7]:

$$\frac{T_{x_{ik}}}{T_{d_k}} = \pi_{t_k}^{-\frac{\gamma-1}{\gamma}} \tag{6}$$

where $\gamma = c_p/c_v$ is the heat capacity ratio, and $k = \{LP, HP\}$. However, the actual turbine deviates from the isentropic idealization, which can be accounted by the isentropic efficiency $\eta_{t_{ik}}$ as follows [25]:

$$\eta_{t_{ik}} \cong \frac{h_{d_k} - h_{x_k}}{h_{d_k} - h_{x_{ik}}} \tag{7}$$

From (6) and (7), and assuming that the actual pressure ratio of a turbine is approximately equal to its nominal value times the air flow rate in p.u. [28]–[30], the exhaust temperature of the high-pressure and low-pressure expanders in p.u. can be calculated as follows:

$$\overline{T}_{x_k} = \frac{T_{d_{ko}} \overline{T}_{d_k}}{T_{x_{ko}}} \left\{ 1 - \left[1 - \frac{1}{\left(\pi_{t_{ko}} \overline{\dot{m}}_t\right)^{\frac{\gamma-1}{\gamma}}} \right] \eta_{t_{ik}} \right\} \tag{8}$$

For a steady-flow, the rate of change of the internal energy of a turbine is zero; hence, the total mechanical power delivered to the generator shaft can be computed as the summation of the difference in rate of change of enthalpy between the inlet and outlet of each expansion stage, as follows:

$$P_{t_m} = \sum_k P_{t_{mk}} = \sum_k \left(\dot{H}_{d_k} - \dot{H}_{x_k} \right) \tag{9}$$

If the enthalpy is expressed as the specific enthalpy times the mass, then the turbine's mechanical power becomes a function of the rate of change of the mass and the temperature difference between the turbine's inlet and outlet. Hence, assuming friction losses represented by the mechanical efficiency $\eta_{t_{mk}}$, the output mechanical power of each expansion stage, in p.u.of the total nominal turbine power, can be approximated by:

$$\overline{P}_{t_{mk}} = \left(\frac{\eta_{t_{km}} c_p \dot{m}_{t_o}}{10^3 P_{t_{mo}}} \right) \overline{\dot{m}}_t \left(T_{d_{ko}} \overline{T}_{d_k} - T_{x_{ko}} \overline{T}_{x_k} \right) \tag{10}$$

where $T_{d_{ok}}$ and $P_{t_{mo}}$ are turbine's parameters; $T_{x_{ko}}$ can be found by solving (8) for $\overline{T}_{d_k} = 1$, $\overline{T}_{x_k} = 1$, and $\overline{\dot{m}}_t = 1$; and $\dot{m}_{t_o}$ can be found by solving (9) and (10) for $P_{t_m} = P_{t_{mo}}$.

4) Synchronous Generator: The synchronous generator model is well-defined in the literature. One of the most commonly used models for dynamic studies is the classical subtransient model, which is described in detail in [31].

5) Control System: The control system proposed for the expansion stage is shown in Fig. 2, and is based on the models presented in [28], [30], and [32] for traditional GTs. This control considers a speed controller (governor) and a low-pressure exhaust temperature controller. The governor uses

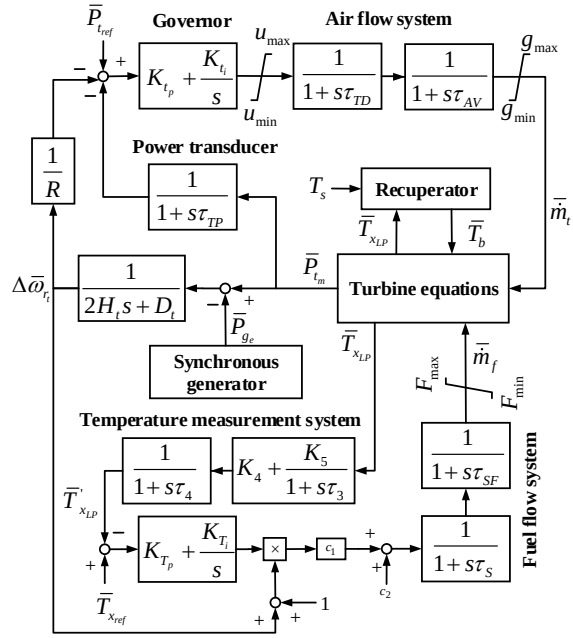

Fig. 2. Control system for CAES expansion stage.

the speed deviation signal $\Delta\overline{\omega}_{r_t}$ in a negative feedback loop to modify the power reference $\overline{P}_{t_{ref}}$ (set manually or by an external AGC signal) creating a steady-state error in the speed, according to the proportional gain $1/R$ (regulation characteristic). The modified power reference is compared with a measured mechanical output power using a power transducer, and the error is passed through a PI controller (governor) which can be tuned to provide good tracking error while achieving a desired dynamic response. The output of the governor is fed into the air flow system, which is modeled by two first-order transfer functions, with time constants τ_{TD} and τ_{AV} representing the turbine's discharge delay, and the valve air opening system including its limits, correspondingly.

The fuel control branch compares the measured low-pressure exhaust temperature signal $\overline{T}'_{x_{LP}}$ to a reference temperature $\overline{T}_{x_{ref}}$, and the error is processed by another PI compensator that controls the fuel system. The temperature measurement system comprises a thermocouple and a radiation shield. The output signal of the PI controller is multiplied by the p.u. rotor speed before being sent to the fuel system, as the operation of the latter depends on the speed, since it is attached to the rotor shaft as indicated in [30]. This signal is

then multiplied by the gain c_1 and added to the constant c_2, which represents the fuel consumption at no load in p.u.; c_1 compensates for the offset introduced by c_2, and $c_1 + c_2 = 1$.

There are two delays associated with the fuel system, one for the valve positioning system that controls the amount of fuel injected, and the other for the downstream piping and gas distribution manifold, both modeled as first order transfer functions connected in series when the fuel is a gas [32]. The output of the fuel flow system is $\overline{\dot{m}}_f$, and the flow rates $\overline{\dot{m}}_t$ and $\overline{\dot{m}}_f$, and $\overline{T}_b$ are inputs to the burners and expanders modeled using (2), (3), (4), (5), (8)-(10). Voltage control is provided by the excitation system of the synchronous generator.

B. Charging Mode

The components involved in this operational mode are the compressor, intercoolers, aftercooler, and synchronous motor. The model presented next allows frequency regulation by the compressor. The high-pressure compressor is modeled as a multi-stage compression system with an intercooler between each stage, while the low-pressure compression is modeled as a single stage compression [22]; an intercooler is also used between the low- and high-pressure compressors. The index j is used to identify the different compression stages as follows: $j = 1$ for low-pressure stage; $j = 2$ for high-pressure first stage; $j = 3$ for high-pressure second stage; and $j = 4$ for high-pressure third stage.

1) Compressor plus heat exchanger: Using similar expressions as those presented for the turbine, a compression stage can be modeled as a temperature gain $\Gamma_j(\overline{\dot{m}}_c)$ plus a heat exchanger, as depicted in Fig. 3, where:

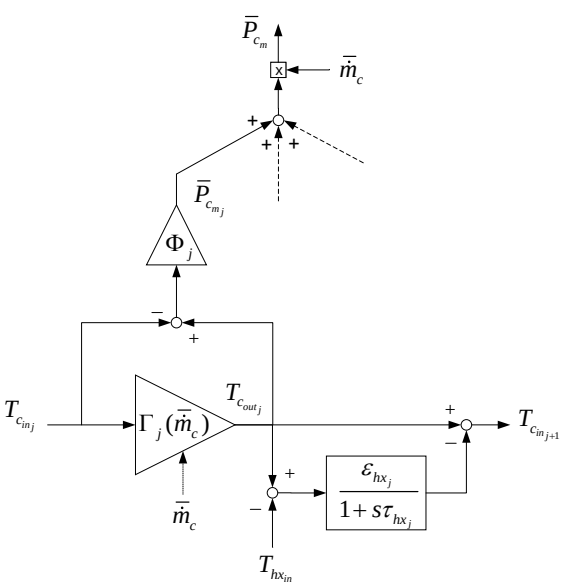

Fig. 3. Model of one compression stage with a heat exchanger at the output.

$$\Gamma_j(\overline{\dot{m}}_c) = 1 + \frac{\left[\pi_{c_j}(\overline{\dot{m}}_c)\right]^{\frac{\gamma-1}{\gamma}} - 1}{\eta_{c_{ij}}} \tag{11}$$

$$\Phi_j = \frac{c_p \overline{\dot{m}}_{c_o}}{10^3 \eta_{c_{mj}} P_{c_{mo}}} \tag{12}$$

The pressure ratio of each compression stage π_{c_j} is a function of the air flow, as determined by a compressor map; here, the compressor map is modeled using the equation of an ellipse, as suggested in [33]. Hence, the pressure ratio of each compressor stage can be calculated as follows:

$$\pi_{c_j}(\overline{\dot{m}}_c) = a_{1_j}\sqrt{1 - \frac{\overline{\dot{m}}_c}{a_{2_j}}} \tag{13}$$

$$\pi_{c_j}(\overline{\dot{m}}_{c_o}) = \pi_{c_{j_o}} \tag{14}$$

$$\pi_{c_j}(0.5\overline{\dot{m}}_{c_o}) = 1.12\pi_{c_{j_o}} \tag{15}$$

Equations (14)-(15) represent two operating points in the compressor map, and are used to find its parameters a_{1_j} and a_{2_j}. In Fig. 3, $\overline{P}_{c_{mj}}$ is the mechanical power consumed by the compressor at the stage j in p.u. of the total nominal compressor power, and $\overline{P}_{c_m}$ is the total mechanical power consumed by the compressor in p.u.; $T_{c_{in_j}}$ and $T_{c_{out_j}}$ are the inlet and outlet temperatures of a compressor stage respectively. The heat exchangers of stages $j = 1, 2, 3$ represent intercoolers, and are modeled with effectiveness ϵ_{hx_j} and time constant τ_{hx_j}. The inlet temperature at the cold side of all heat exchangers $T_{hx_{in}}$ is the same, and remains constant assuming that the heat capacity rate of the cooling fluid (water) is much higher than the compressor air flow's heat capacity rate. The aftercooler corresponds to the heat exchanger of stage $j = 4$.

2) Synchronous Motor: The synchronous motor is modeled using the same subtransient model as the synchronous generator [31], with the motor driving the mechanical load (compressor).

3) Control System: As illustrated in Fig. 4, the mechanical power required by the compressor depends on the air flow rate, which is controlled by moving the variable inlet guide vanes. A feedback of the rotor's speed deviation modifies the reference power $\overline{P}_{c_{ref}}$, as in the generator case; however, the sign of this feedback is positive in the governor loop, because the compressor has to decrease its power consumption when the frequency drops, and do the opposite when the frequency increases. The error between the measured power and the modified reference power is passed through a PID governor which sends the signal to the IGVs, whose operation is assumed to be linear with respect to $\overline{\dot{m}}_c$.

The air flow dynamics due to mass flow accumulation at each compression stage are very fast, hence, their combined effect is modeled by a single transfer function with time constant τ_{CD} [32]. The output of this series arrangement of transfer functions is multiplied by the rotor speed to obtain $\overline{\dot{m}}_c$, since the actual air flow depends on the rotational speed of the compressor. Unlike the turbine, the discharge temperature of the compressor is not controlled, and l_{min} and l_{max} are limits in the air flow to prevent the compressor from operating in surge or choke conditions (usually 60% to 100% of the nominal air flow). Finally, $\overline{\dot{m}}_c$ is used as input to the compressor stages, as shown in Fig. 3. The voltage control is provided using the same model as for the generator.

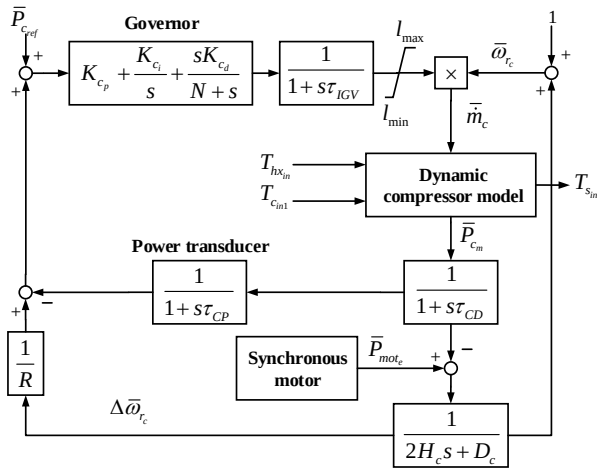

Fig. 4. Control system for CAES compression stage.

C. Simplified Model of CAES System

1) Expansion: As is typically done in gas turbines to simplify their mechanical model, the HP and LP expansion stages can be approximated by a single stage [33]. Thus, assuming that the low-pressure and high-pressure expansion stages have the same pressure ratio, and adding the reheating effect of the low-pressure burner, the CAES turbine exhaust temperature can be calculated as follows:

$$\overline{T}_x = \frac{T_{d_o}\overline{T}_d + \Delta T_o\left(\frac{\overline{\dot{m}}_f}{\overline{\dot{m}}_t}\right)}{T_{x_o}}\left\{1 - \left[1 - \frac{1}{\left(\pi_{t_o}\overline{\dot{m}}_t\right)^{\frac{\gamma-1}{2\gamma}}}\right]\eta_{t_i}\right\} \tag{16}$$

where $\pi_{t_o} = \pi_{t_{LPo}}\pi_{t_{HPo}}$ is the total expansion pressure ratio. The term $\Delta T_o\left(\frac{\overline{\dot{m}}_f}{\overline{\dot{m}}_t}\right)$ represents the inlet low-pressure temperature rise due to the low-pressure burner. The total mechanical output power can then be calculated as follows:

$$\overline{P}_{t_m} = \frac{\eta_{t_i}\eta_{t_m}c_p\dot{m}_t\left(2T_d + \Delta T_o\left(\frac{\overline{\dot{m}}_f}{\overline{\dot{m}}_t}\right)\right)}{10^3 P_{t_{mo}}}\left\{1 - \frac{1}{\left(\pi_{t_o}\overline{\dot{m}}_t\right)^{\frac{\gamma-1}{2\gamma}}}\right\} \tag{17}$$

where η_{t_i} and η_{t_m} are the equivalent mechanical and isentropic efficiency of the expansion correspondingly. The recuperator, high-pressure burner (now referred to as burner), and control system remain the same as in the detailed model, substituting T_x for $T_{x_{LP}}$, and T_d for $T_{d_{HP}}$.

2) Compression: The high-pressure multi-stage compressor can be reduced to a single-stage compressor, assuming ideal operation of the intercoolers, which would keep the inlet temperature of each stage equal to the inlet condition of the first high-pressure stage (isothermal compression) [34]. Under these assumptions, the CAES compressor could be modeled using two stages of the compression-heat-exchanger illustrated in Fig. 3, with $j = 1$ representing the low-pressure compressor, and $j = 2$ the high-pressure compressor. Hence, the temperature gain $\Gamma_2(\overline{\dot{m}}_c)$ and compressor's stage power constant Φ_2 become:

$$\Gamma_2(\overline{\dot{m}}_c) = 1 + \frac{\left[\pi_{c_2}(\overline{\dot{m}}_c)\right]^{\frac{\gamma-1}{3\gamma}} - 1}{\eta_{c_{i2}}} \tag{18}$$

$$\Phi_2 = \frac{3c_p\overline{\dot{m}}_{c_o}}{10^3\eta_{c_{m_2}}P_{c_{mo}}} \tag{19}$$

to account for the reduction of the three compressor stages. In this case, π_{c_2} is the total pressure ratio of the high-pressure compressor, $\eta_{c_{m2}}$ is the total mechanical efficiency, and $\eta_{c_{i2}}$ is the equivalent isentropic efficiency of the single stage high-pressure compressor. The heat-exchanger for stage $j = 2$ represents the aftercooler in this model, whereas the low-pressure compressor ($j = 1$), electrical motor, and control system remain the same as in the detailed model. The equivalent simplified CAES facility is shown in Fig. 5.

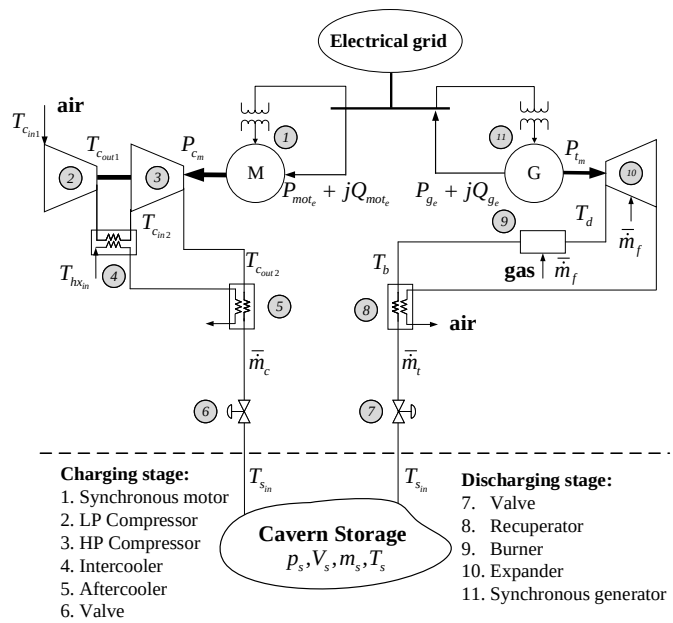

Fig. 5. Simplified CAES model.

D. Cavern Model

From the conservation of mass in an open system considering the cavern as a control volume, the mass in p.u. can be calculated as follows:

$$\overline{\dot{m}}_s = \frac{1}{m_{s_o}}\left(\overline{\dot{m}}_c\dot{m}_{c_o} - \overline{\dot{m}}_t\dot{m}_{t_o}\right) \tag{20}$$

$$m_{s_o} = \frac{10^5 p_{s_o}V_s}{\mathrm{R}T_s} \tag{21}$$

From the conservation of energy and the state equation defined by the Ideal Gas Law, the pressure for an adiabatic and isochoric cavern can be calculated as follows [9]:

$$\dot{\overline{p}}_s = \frac{\mathrm{R}\gamma}{10^5\,V_s\,p_{s_o}}\left(\overline{\dot{m}}_c\dot{m}_{c_o}\overline{T}_{s_{in}}T_{s_{ino}} - \overline{\dot{m}}_t\dot{m}_{t_o}T_s\right) \tag{22}$$

Since the proposed dynamic model is developed to study the CAES system for about 200 s, it is assumed here that the internal temperature of the cavern T_s remains constant during the period of analysis. In these equations, the pressure and mass are expressed in p.u. of the cavern's nominal values. The initial conditions for the integration of $\overline{m}_s$ and $\overline{p}_s$ are $\overline{m}_{s_{ref}}$ and $\overline{p}_{s_{ref}}$, respectively.

IV. Results and Discussion

In this section, step changes in the reference values are first simulated, with results being compared to the models proposed in [15] and [16]. Since the proposed CAES system model is highly nonlinear and comprises several dynamic sub-systems and controls, such as temperature control, heat exchangers, measurement systems, etc., step-changes are used to study the controls and system dynamic responses without external disturbances, and to highlight the differences with respect to existing models. Then, operation of the proposed CAES system models is compared with a traditional GT model and the simplified model in [15] to provide frequency regulation for a grid with high penetration of wind generation. Parameters of the CAES Huntorf plant available from [6], [22], [35], [36] and [37] were used in the presented simulations; the corresponding dynamic data was taken from [27], [30], [32], [35], and [38], and the turbomachinery inertias were obtained from [39]. The isentropic efficiencies of the expansion stages and high-pressure compression stage were calculated for nominal turbine and compressor conditions. The gains of the PI and PID controllers were obtained by trial and error to produce the best possible dynamic response of the CAES system. All parameters used in the simulations are shown in Table I.

TABLE I
CAES and System Parameters

Parameter	Value	Parameter	Value	Parameter	Value
Discharging mode					
$T_{d_{HPo}}[K]$	823.15	$T_{d_{LPo}}[K]$	1098.2	$T_{x_{HPo}}[K]$	612.15
$T_{x_{LPo}}[K]$	668.15	$\pi_{t_{HPo}}$	3.818	$\pi_{t_{LPo}}$	10.856
$\eta_{t_{HPm}}[p.u.]$	0.99	$\eta_{t_{LPm}}[p.u.]$	0.99	$\eta_{t_{HPi}}[p.u.]$	0.8065
$\eta_{t_{LPi}}[p.u.]$	0.7926	$T_{b_o}[K]$	599.15	$\epsilon_r[p.u.]$	0.80
$c_p[kJ/kg.K]$	1.055	$P_{t_{mo}}[MW]$	280	γ	1.4
$\dot{m}_{t_o}[kg/s]$	417	$\dot{m}_{f_o}[kg/s]$	12	$\tau_R[s]$	25
K_4	0.8	K_5	0.2	$\tau_3[s]$	15
$\tau_4[s]$	2.5	K_{T_p}	7	K_{T_i}	5
$\tau_S[s]$	0.05	$\tau_{SF}[s]$	0.4	$F_{max}[p.u.]$	1.25
$F_{min}[p.u.]$	0	$c_2[p.u.]$	0.05	$\tau_{AV}[s]$	0.1
$\tau_{TD}[s]$	0.3	$g_{max}[p.u.]$	1.25	$g_{min}[p.u.]$	0.1
$R[p.u.]$	0.04	K_{t_p}	3	K_{t_i}	2
$\tau_{TP}[s]$	0.02	$u_{max}[p.u.]$	1.2	$u_{min}[p.u.]$	0
$H_t[s]$	3.9821	$D_t[p.u]$	2	$K_{AGC_2}[p.u.]$	60
Discharging mode simplified model					
Parameter	Value	Parameter	Value	Parameter	Value
$\Delta T_o[K]$	315.73	$T_{x_o}[K]$	762.41	$\eta_{t_i}[p.u.]$	0.7995
$\eta_{t_m}[p.u.]$	0.9801	π_{t_o}	41.451		
Charging mode					
Parameter	Value	Parameter	Value	Parameter	Value
$T_{c_{in1}}[K]$	283.15	$T_{c_{out1o}}[K]$	497.6	ϵ_{hx_1}	0.8785
$T_{c_{in2o}}[K]$	323.15	$T_{c_{out2o}}[K]$	420.5	ϵ_{hx_2}	0.8
$T_{c_{in3o}}[K]$	323.15	$T_{c_{out3o}}[K]$	421.5	ϵ_{hx_3}	0.8
$T_{c_{in4o}}[K]$	323.15	$T_{c_{out4o}}[K]$	421.2	ϵ_{hx_4}	0.8
$\eta_{c_{i1}}[p.u.]$	0.8200	$\eta_{c_{m1}}[p.u.]$	0.99	$\pi_{c_{1o}}$	5.4290
$\eta_{c_{i2}}[p.u.]$	0.9115	$\eta_{c_{m2}}[p.u.]$	0.99	$\pi_{c_{2o}}$	2.3460
$\eta_{c_{i3}}[p.u.]$	0.9023	$\eta_{c_{m3}}[p.u.]$	0.99	$\pi_{c_{3o}}$	2.3460
$\eta_{c_{i4}}[p.u.]$	0.9097	$\eta_{c_{m4}}[p.u.]$	0.99	$\pi_{c_{4o}}$	2.3460
$\tau_{hx_1}[s]$	12	$\tau_{hx_2}[s]$	12	$\tau_{hx_3}[s]$	12
$\tau_{hx_4}[s]$	12	$H_c[s]$	12.957	$D_c[p.u.]$	0
$P_{c_{mo}}[MW]$	58.7	γ	1.4	$c_p[kJ/kg.K]$	1.055
$T_{hx_{in}}[K]$	298.7	$R[p.u.]$	0.04	K_{c_d}	0.214
K_{c_p}	0.4147	K_{c_i}	0.1485	$N[rad/s]$	1.0792
$\tau_{CD}[s]$	0.2	$\tau_{IGV}[s]$	0.2	$l_{max}[p.u.]$	1.15
$l_{min}[p.u.]$	0.6	$\tau_{Dr}[s]$	1.5	$\tau_{CP}[s]$	0.02
$K_{droop}[p.u.]$	2000	$\dot{m}_{c_o}[kg/s]$	108		
Charging mode simplified model					
Parameter	Value	Parameter	Value	Parameter	Value
$\pi_{c_{2o}}$	12.9117	$\eta_{c_{i2}}[p.u.]$	0.9142	$\eta_{c_{m2}}[p.u.]$	0.9703
Cavern					
Parameter	Value	Parameter	Value	Parameter	Value
$p_{s_o}[bar]$	42	$V_s[m^3]$	300000	$T_s[K]$	323.15
R$[J/kg.K]$	287.058				
System					
Parameter	Value	Parameter	Value	Parameter	Value
$P_{GTo}[MW]$	213.4	$P_{ST1o}[MW]$	200	$P_{ST2o}[MW]$	200
$P_{wo}[MW]$	200	$H_{GT}[s]$	18.5	$H_{ST1}[s]$	3.17
$H_{ST2}[s]$	3.17	$H_w[s]$	3	$K_{AGC_1}[p.u.]$	20

A. Dynamic Performance Studies

A 280 MW turbine and 60 MW compressor supplying/consuming 0.7 p.u. power, respectively, were simulated in Matlab/Simulink. Step changes of +0.3, -0.3, -0.1, +0.1, +0.5, and -0.5 p.u. were respectively applied at t = 5s, 20s, 35s, 50s, 65s, and 80s in the turbine power reference; and at t = 5s, 30s, 60s, 80s, 120s, and 140s in the compressor power reference of both the proposed models, detailed and simplified. In both cases, the speed deviation feedback with the permanent droop characteristic R is disconnected. The response of these models is also compared with two existing CAES models described in [15] and [16], with the primary-frequency control feedback disabled in [15], and not considering the converters interfacing the grid in [16], but representing the storage controller with the mechanical power generated/consumed by the CAES system as its input signal; the PI controller parameters of the latter were also tuned to obtain the best dynamic performance. The dynamic response of the compression and expansion stages are shown in Fig. 6 and Fig. 7, respectively.

In Fig. 6, observe that, even though the simplified model considers only the dynamics of one intercooler, it has a very similar response to the detailed model. This is due to three factors. First, the airflow is almost equal at each stage of compression, as discussed in Section III-B3. Second, the output temperature of the intercooler at stage $j+1$ is directly affected by the instantaneous change of the output temperature of the previous stage j, which is then modified slowly as the heat is removed. Finally, each compression stage contributes to the total consumed power independently, as shown in Fig. 3. Notice that for every step change there is a fast transient in the proposed models produced by the rapid change in the air flow, and the initial response of the intercoolers. At time t = 130s, the air flow reaches its maximum limit; however, a dropping airflow is observed because the actual air flowing through the compressor is a function of the rotor speed, as shown in Fig. 4. Observe that no control action was taken on the compressor's discharge temperature; hence, the temperatures at the different stages present similar transients as $\overline{\dot{m}}_c$, as shown in Fig. 6(c). The input temperatures to the cavern $T_{s_{in}}$ in the detailed and simplified models are similar in steady-stage, although some

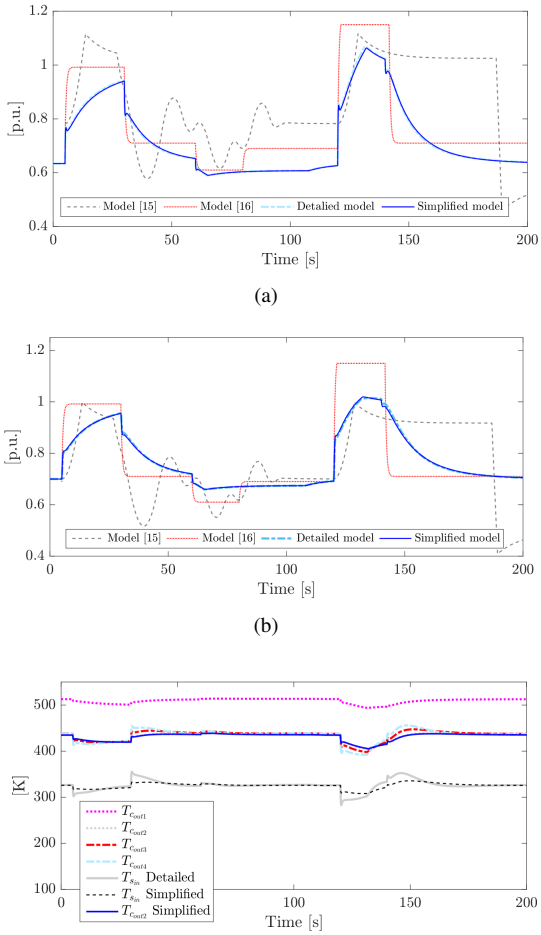

Fig. 6. Dynamic response of CAES compressor to step changes in power reference: (a) air flow, (b) active power, and (c) stage temperatures.

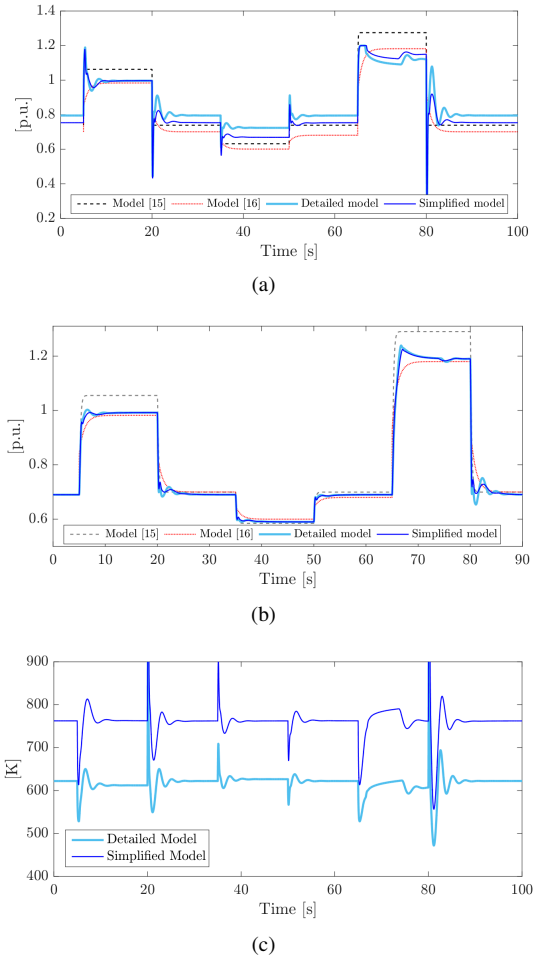

Fig. 7. Dynamic response of CAES expander to step changes in power reference: (a) air flow, (b) active power, and (c) exhaust temperatures.

differences can be noticed during the transients; however, these differences are not big enough to affect the state of charge of the cavern because of the large size of the cavern.

Models from [15] and [16] show significant differences in their transient response in compression mode with respect to the proposed models. This is because the model in [16] ignores the dynamics associated with physical components of CAES such as heat exchangers, and explicitly represents only the rotational inertia and the cavern pressure. As such, [16]'s compressor model responds very rapidly in this case according to the storage controller parameters. This model does not include limits in the air flow either; therefore, the airflow is much larger in the interval of 120 to 140s. The model in [15], on the other hand, uses a rate-of-change limiter that prevents the compressor from changing its operating point too fast; however, only the dynamics of the air-adjusting valve are represented, which makes their response faster than the models proposed here, and also more oscillatory.

The turbine response illustrated in Fig. 7 is more uniform than that of the compressor, in all tested models. One noticeable difference between the proposed models and those in [15] and [16] is the magnitude of the air flow transients and power; this is due to the combined effect of the burner models and the temperature controller, not represented in [15] and [16]. As can be seen in Fig. 7(c), the temperature controller keeps the low pressure exhaust temperature at its reference value, regardless of the airflow or power consumed by the compressor, introducing delays in the mechanical output power of the turbine; however, the action of the controller determines that the fuel flow should be either increased or decreased suddenly, which modifies the composition of air-gas in the burner, thus affecting the amount of air required to realize the reference output power. Observe the negative overshoots in the exhaust temperature due to the increasing air inflow cooling down the burners. Finally, the model from [16] does not consider the physical dynamics in the turbine, thus its response is also very fast. Similarly, in [15], the dynamics of the recuperator are not modeled, leaving the governor and the pressure valve delays as the only two dynamic components in the model; hence, the response of the turbine is mostly defined by the governor and pressure valve time constants, which are small.

The mechanical power obtained using the proposed detailed and simplified models are similar; therefore, either could be used for electrical grid studies, since the mechanical power is the main interface with the electrical system (synchronous

generator). Only the magnitude of the transients presents some differences between these models; however, the steady-state magnitudes of the airflow and temperature present some differences due to the assumption of equal pressure ratios in the high and low-pressure expanders.

Note that a clear advantage of the simplified model is a reduction in the amount and detail of the parameters required. Thus, in the detailed model, the input and output temperatures, efficiency, effectiveness and time constants of heat exchangers, pressure ratios, etc., must be specified for each compression/expansion stage. The required information may be unavailable or may require extensive machine testing and measurements. Estimating these parameters is complicated due to the interrelations between variables within the different stages; furthermore, initializing the model is cumbersome. On the other hand, the proposed simplified CAES model involves fewer parameters because of the lumped representation used in this model, such as the nominal pressure ratio of the HP compressor or the inlet temperature of the turbine. Moreover, the complexity of the parameter estimation is reduced as several internal variable relations are avoided.

B. Frequency Regulation

The power system model shown in Fig. 8 is used to study the impact of CAES in frequency regulation; the electrical system is approximated by transfer functions, since the system dynamic responses are much faster than the mechanical systems which are represented in some detail in the model and more significantly impact the system's frequency response. The test system comprises relevant and realistic models of different generation technologies, and configuring the system to have 33% of the load being supplied by wind generation, which is the main source of frequency disturbance. Steam and gas generators were sized to be able to supply the demand even when the wind power goes to zero, with corresponding realistic dynamic data. The base case (Case 1) comprises a fixed load of 650 MW, a 200 MW wind farm, two 200 MW steam turbine units contributing to primary frequency regulation, and a 213.4 MW gas turbine (GT) that provides primary and secondary frequency regulation. Secondary control is added by integrating the speed deviation, which emulates a traditional Automatic Generation Control (AGC). In Case 2, one steam turbine units is replaced by a 280 MW-discharging/ 60 MW-charging CAES system, which operates in discharging mode only. Finally, in Case 3, the CAES system operates in simultaneous charging and discharging modes.

The initial conditions for the three cases are summarized in Table II. The system is in steady-state at 60 Hz nominal frequency before $t = 30\,s$. The gains $K_{AGC_1} = 20$, and $K_{AGC_2} = 60$ for the GT and CAES turbine, respectively, were tuned to achieve the best frequency performance; furthermore, in order to improve the response of the compressor, a transient droop control was added, as shown in Fig. 8. The wind farm is comprised of a simple aggregation of 100 2-MW Doubly-Fed Induction Generators (DFIG), based on the models reported in [40] and [41]. The wind profile was artificially created using a Weibull distribution (shape parameter k=2, and scale parameter Λ = 12.1505), which was smoothed out with a low-pass filter [42]. The steam turbine model and parameters were taken from [31]. The model proposed in [32] was used for the GT, excluding the acceleration control and assuming the use of gas as fuel.

TABLE II
INITIAL CONDITIONS FOR SIMULATED CASES

	Case 1	Case 2	Case 3
Steam generation [MW]	350	175	175
Wind generation [MW]	200	200	200
GT generation [MW]	100	100	100
CAES generation [MW]	-	175	221.96
CAES compressor load [MW]	-	-	46.96

A comparison of the system frequency for Cases 1, 2, and 3 for the proposed detailed and simplified CAES models are presented in Fig. 9 (a). The normal and abnormal operation limits are as per the Ontario's Independent Electricity System Operator (IESO) [43]. The results show very similar frequency responses for the simplified and detailed CAES models in Cases 2 and 3; the main difference is the magnitude of the frequency excursions, which, as discussed in Section IV-A, are better captured by the detailed model. The largest error in the frequency deviation between the simplified and detailed models is 0.03 Hz (0.05%). The simplified model had the additional advantage of requiring less than half as much time to simulate as did the corresponding more detailed model (17.8s vs. 38.8s for Case 3). Observe that the combined operation of compressor and turbine in Case 3 produces a better frequency regulation than Cases 1 and 2. Thus, the maximum positive frequency excursion is reduced from 60.39 Hz in Case 1, to 60.17 Hz in Case 2, and 60.16 Hz in Case 3; and the largest negative frequency excursion decreases from 59.68 Hz, to 59.89 Hz, and 59.89 Hz, respectively. Furthermore, for the considered simulation period, in Case 3 the combined charging and discharging is more effective in flattening out the frequency than in the other two cases; this can be attributed to the operation of the compressor using the proposed transient droop control, and the inertia added by the rotating masses of the compressor and synchronous motor. Similarly, the number of frequency excursions beyond limits is reduced from 5 to 0 when comparing Case 1 to Cases 2 or 3.

In Fig. 9 (b), the cumulative absolute value of frequency deviation is used as a quantitative measurement of the performance of each alternative considered. Note that the detailed model yields a larger cumulative frequency deviation than the reduced model in both Cases 2 and 3; thus, the difference between the two models for Case 2 is around 20%, while it is 10% for Case 3. Nevertheless, from this metric, it can be concluded that Case 2 is better than Case 1, and Case 3 is better than the other two. At the end of the simulation time, comparing the results of the detailed models, the value for Case 2 is 58.89% of that in Case 1, and 31.98% for Case 3 with respect to Case 1. A quasi-linear trend is observed in the three plots; thus, the relative proportion of this metric is expected to remain constant in time.

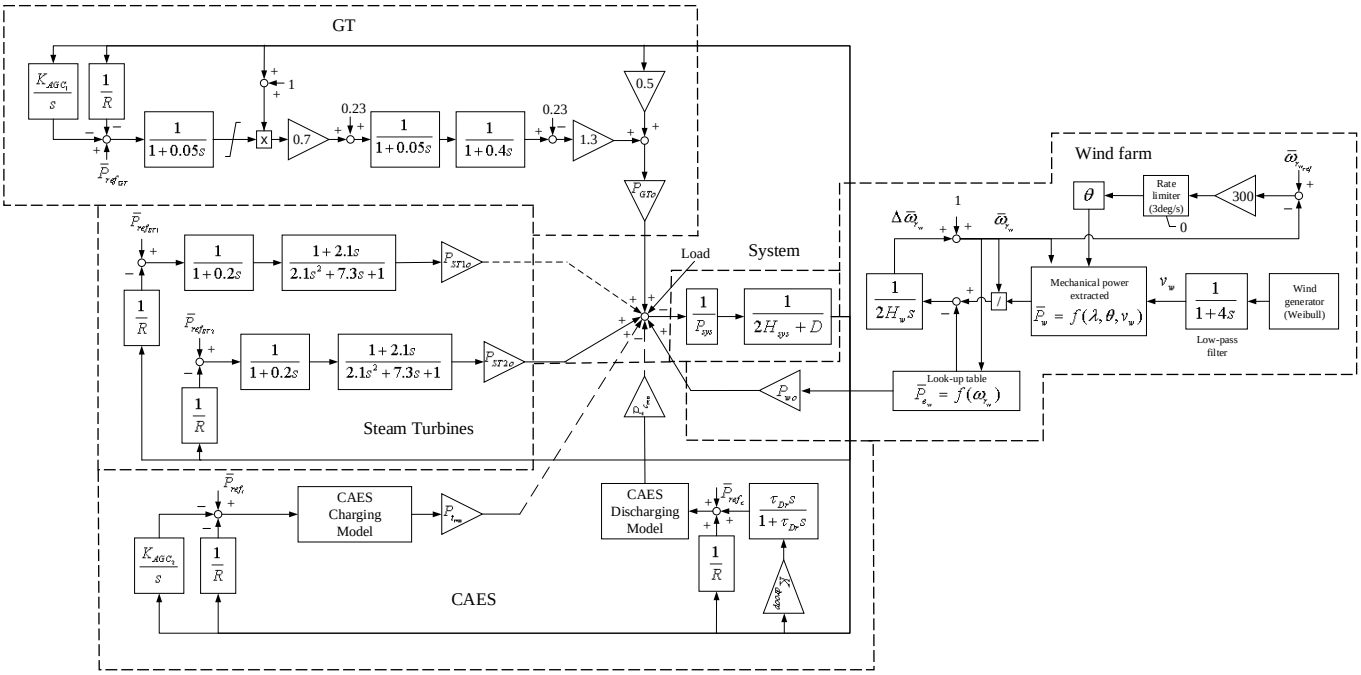

Fig. 8. System configuration for frequency regulation studies with CAES.

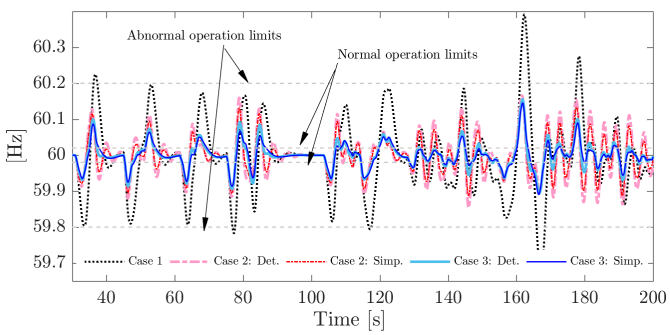

(a)

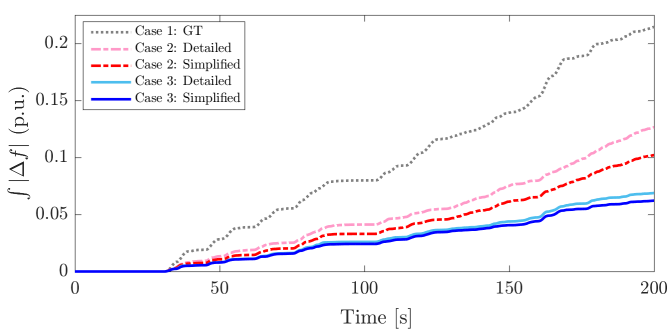

(b)

Fig. 9. Frequency (a) plots and (b) regulation performance for all three cases.

Fig. 10 shows a comparison of the proposed CAES models and the model in reference [15] for Case 3. It is important to mention that if $K_{AGC_2} = 60$ is used for the CAES charging model from [15], the system is unstable; therefore, the gain was reduced to $K_{AGC_2} = 10$. As highlighted before, observe

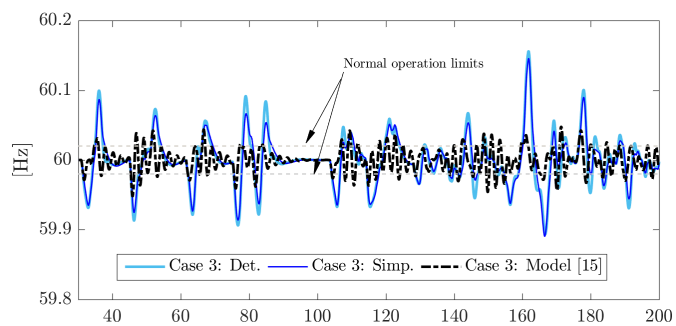

Fig. 10. System frequency for Case 3.

that because the model in [15] neglects some dynamics, its response is much faster, resulting in smaller frequency deviations.

V. Conclusion

In this paper, a detailed mathematical model of the diabatic CAES system and a simplified version were proposed, which consider two independent synchronous machines properly interfaced with the mechanical subsystems. The two models were tested for step changes in their power reference values and frequency regulation studies, showing similar responses; however, the simplified model requires fewer parameters and less simulation time as compared to the detailed model, which makes the former preferable when modeling CAES systems connected to a bulk power system. If a more accurate assessment of frequency deviation were required, the detailed model should be used.

Even though deployment of a CAES facility need be justified in the energy arbitrage market, added value could

be obtained in other markets, such as the ancillary service market. In particular, it was demonstrated in this paper that a CAES connected to a power system could provide frequency regulation, operating in simultaneous charging and discharging modes, contributing to significantly reduce the cumulative frequency deviation of the system. This is only possible in a configuration with independent generator and motor machines, as proposed here. Future work includes implementing and testing the proposed models in a benchmark power system for realistic transient and frequency stability studies.

REFERENCES

[1] B. Cleary, A. Duffy, A. O'Connor, M. Conlon, and V. Fthenakis, "Assessing the economic benefits of compressed air energy storage for mitigating wind curtailment," *IEEE Trans. Sustain. Energy*, vol. 6, no. 3, pp. 1021–1028, 2015.

[2] "EPRI-DOE handbook of energy storage for transmission & distribution applications," Tech. report, EPRI and U.S. Department of Energy, Palo Alto, CA, and Washington, DC, pp. 3–35, 2003.

[3] J. Konrad, R. Carriveau, M. Davison, F. Simpson, and D. S.-K. Ting, "Geological compressed air energy storage as an enabling technology for renewable energy in Ontario, Canada," *Int. J. Environmental Stud.*, vol. 69, no. 2, pp. 350–359, 2012.

[4] J. Simmons, A. Barnhart, S. Reynolds, and S. Young-Jun, "Study of compressed air energy storage with grid and photovoltaic energy generation," Tech. report, The Arizona Research Institute for Solar Energy (AzRISE)-APS, 2010. [Online]. Available: http://u.arizona.edu/$\sim$sreynold/caes.pdf

[5] S. Succar and R. H. Williams, "Compressed air energy storage: theory, resources, and applications for wind power," Tech. report, Princeton Environmental Institute, 2008. [Online]. Available: https://acee.princeton.edu/wp\-content/uploads/2016/10/SuccarWilliams_PEI_CAES_2008April8.pdf

[6] "Huntorf air storage gas turbine power plant," Tech. report No. D GK 90 202 E, Brown Boveri (BBC), Germany. [Online]. Available: www.solarplan.org/Research/BBC_Huntorf_engl.pdf

[7] P. Zhao, L. Gao, J. Wang, and Y. Dai, "Energy efficiency analysis and off-design analysis of two different discharge modes for compressed air energy storage system using axial turbines," *Renewable Energy*, vol. 85, pp. 1164–1177, 2016.

[8] Y. Mazloum, H. Sayah, and M. Nemer, "Static and dynamic modeling comparison of an adiabatic compressed air energy storage system," *J. Energy Resources Technol.*, vol. 138, no. 6, p. 062001, 2016.

[9] W. He, X. Luo, D. Evans, J. Busby, S. Garvey, D. Parkes, and J. Wang, "Exergy storage of compressed air in cavern and cavern volume estimation of the large-scale compressed air energy storage system," *Applied Energy*, vol. 208, pp. 745–757, 2017.

[10] T. Xia, L. He, N. An, M. Li, and X. Li, "Electromechanical transient modeling research of energy storage system based on power system security and stability analysis," in *IEEE Int. Conf. on Power Syst. Technol. (POWERCON)*, Chengdu, China, 2014, pp. 221–226.

[11] L. He, T. Xia, F. Tian, and N. An, "Modeling and simulation of compressed air energy storage (CAES) system for electromechanical transient analysis of power system," *Advanced Materials Research*, vol. 860, pp. 2486–2494, 2014.

[12] M. V. Dahraie, H. Najafi, R. N. Azizkandi, and M. Nezamdoust, "Study on compressed air energy storage coupled with a wind farm," in *IEEE 2nd Iranian Conf. on Renewable Energy and Distributed Generation (ICREDG)*, Tehran, Iran, 2012, pp. 147–152.

[13] H. T. Le and S. Santoso, "Increasing wind farm transient stability by dynamic reactive compensation: Synchronous-machine-based ESS versus SVC," in *IEEE Power and Energy Society General Meeting*, Minneapolis, MN, 2010, pp. 1–8.

[14] ——, "Operating compressed-air energy storage as dynamic reactive compensator for stabilising wind farms under grid fault conditions," *IET Renewable Power Generation*, vol. 7, no. 6, pp. 717–726, 2013.

[15] I. Kandiloros and C. Vournas, "Use of air chamber in gas-turbine units for frequency control and energy storage in a system with high wind penetration," in *IEEE PES Innovative Smart Grid Technol. Conf. Europe (ISGT-Europe)*, Istanbul, Turkey, 2014, pp. 1–6.

[16] A. Ortega and F. Milano, "Generalized model of VSC-based energy storage systems for transient stability analysis," *IEEE Trans. Power Syst.*, vol. 31, no. 5, pp. 3369–3380, 2016.

[17] N. Hasan, M. Y. Hassan, M. S. Majid, and H. A. Rahman, "Mathematical model of compressed air energy storage in smoothing 2MW wind turbine," in *IEEE Int. Power Eng. and Optimization Conf. (PEDCO)*, Melaka, Malaysia, 2012, pp. 339–343.

[18] Z. Xiaoshu and Z. Hong, "Switched reluctance motor/generator simulation research based on compressed air energy storage system," in *Int. Conf. on Advanced Mechatronic Syst. (ICAMechS)*, Beijing, China, 2015, pp. 479–484.

[19] M. Martínez, M. Molina, and P. Mercado, "Dynamic performance of compressed air energy storage (CAES) plant for applications in power systems," in *IEEE PES Transmission and Distribution Conf. and Expo.: Latin America (T&D-LA)*, Sao Paulo, Brazil, 2010, pp. 496–503.

[20] "SMARTCAES Compressed Air Energy Storage Solutions," Brochure, DRESSER-RAND, 2015. [Online]. Available: www.dresser-rand.com

[21] H. Daneshi, A. Srivastava, and A. Daneshi, "Generation scheduling with integration of wind power and compressed air energy storage," in *IEEE PES Transmission and Distribution Conf. and Expo.*, New Orleans, LA, 2010, pp. 1–6.

[22] B. J. Davidson, I. Glendenning, R. D. Harman, A. B. Hart, B. J. Maddock, R. D. Moffitt, V. G. Newman, T. F. Smith, P. J. Worthington, and J. K. Wright, "Large-scale electrical energy storage," *IEE Proc. A - Physical Science, Measurement and Instrumentation, Management and Education - Reviews*, vol. 127, no. 6, pp. 345–385, 1980.

[23] R. B. Schainker and M. Nakhamkin, "Compressed-air energy storage (CAES): Overview, performance and cost data for 25MW to 220MW plants," *IEEE Trans. Power App. Syst.*, no. 4, pp. 790–795, 1985.

[24] K. Allen, "CAES: The underground portion," *IEEE Trans. Power App. Syst.*, vol. PAS-104, no. 4, pp. 809–812, July 1985.

[25] Y. Cengel and M. Boles, *Thermodynamics: An Engineering Approach*. 8th ed., NY: McGraw-hill, 2002.

[26] T. L. Bergman and F. P. Incropera, *Fundamentals of heat and mass transfer*. 6th ed., NY: John Wiley & Sons, 2007.

[27] H. A. d. S. Mattos, C. Bringhenti, D. F. Cavalca, O. F. R. Silva, G. B. d. Campos, and J. T. Tomita, "Combined cycle performance evaluation and dynamic response simulation," *Aerosp. Electron. Syst. Mag.*, vol. 8, no. 4, pp. 491–497, 2016.

[28] IEEE Working Group on Prime Mover and Energy Supply Models for System Dynamic Performance Studies, "Dynamic models for combined cycle plants in power system studies," *IEEE Trans. Power Syst.*, vol. 9, no. 3, pp. 1698–1708, Aug 1994.

[29] J. Mantzaris and C. Vournas, "Modelling and stability of a single-shaft combined cycle power plant," *Int. J. Thermodynamics*, vol. 10, no. 2, pp. 71–78, 2007.

[30] N. Kakimoto and K. Baba, "Performance of gas turbine-based plants during frequency drops," *IEEE Trans. Power Syst.*, vol. 18, no. 3, pp. 1110–1115, 2003.

[31] P. Kundur, *Power system stability and control*. NY: McGraw-hill, 1994.

[32] W. I. Rowen, "Simplified mathematical representations of heavy-duty gas turbines," *J. Eng. for Power*, vol. 105, no. 4, pp. 865–869, 1983.

[33] W. Fuls, "Enhancement to the traditional ellipse law for more accurate modeling of a turbine with a finite number of stages," *Journal of Engineering for Gas Turbines and Power*, vol. 139, no. 11, p. 112603, 2017.

[34] P. Vadasz and D. Weiner, "The optimal intercooling of compressors by a finite number of intercoolers," *Journal of Energy Resources Technology*, vol. 114, no. 3, pp. 255–260, 1992.

[35] E. Macchi and G. Lozza, "A study of thermodynamic performance of caes plants, including unsteady effects," in *ASME 1987 International Gas Turbine Conference and Exhibition*, CA, 1987, pp. V004T10A008–V004T10A008.

[36] T. Schobeiri and H. Haselbacher, "Transient analysis of gas turbine power plants, using the Huntorf compressed air storage plant as an example," in *ASME 1985 International Gas Turbine Conference and Exhibit*, Baden, Switzerland, 1985, pp. V003T10A015–V003T10A015.

[37] W. Liu, L. Liu, L. Zhou, J. Huang, Y. Zhang, G. Xu, and Y. Yang, "Analysis and optimization of a compressed air energy storage combined cycle system," *Entropy*, vol. 16, no. 6, pp. 3103–3120, 2014.

[38] N.-b. Zhao, X.-y. Wen, and S.-y. Li, "Dynamic time-delay characteristics and structural optimization design of marine gas turbine intercooler," *Mathematical Problems in Engineering*, vol. 2014, 2014.

[39] P. M. Anderson and A. A. Fouad, *Power system control and stability*. NJ: John Wiley & Sons, 2008.

[40] J. Slootweg, S. De Haan, H. Polinder, and W. Kling, "General model for representing variable speed wind turbines in power system dynamics simulations," *IEEE Trans. Power Syst.*, vol. 18, no. 1, pp. 144–151, 2003.

[41] J. Dang, J. Seuss, L. Suneja, and R. G. Harley, "SoC feedback control for wind and ESS hybrid power system frequency regulation," *IEEE J. Emerging Sel. Topics Power Electron.*, vol. 2, no. 1, pp. 79–86, 2014.
[42] F. Milano, *Power system modelling and scripting*. London: Springer Science & Business Media, 2010.
[43] "Market manual 7: System operations part 7.1: IESO controlled grid operating procedures," Ontario's Independent Electricity System Operator, 2017. [Online]. Available: www.ieso.ca/rules/-/media/ccdae55168cc4ae8a4b73894ba305ebe.ashx

Ivan Calero (S'17)) received the diploma in electrical engineering from Escuela Politécnica Nacional (EPN), Quito, Ecuador, in 2008. He is currently pursuing the Ph.D. degree in Electrical and Computer Engineering with the University of Waterloo, ON, Canada. His research interests include modeling, analysis and control of power systems.

Claudio A. Cañizares (S'85,M'91,SM'00,F'07) is a Full Professor and the Hydro One Endowed Chair at the Electrical and Computer Engineering (E&CE) Department of the University of Waterloo, where he has held various academic and administrative positions since 1993. He received the Electrical Engineer degree from the Escuela Politècnica Nacional (EPN) in Quito-Ecuador in 1984, where he held different teaching and administrative positions between 1983 and 1993, and his MSc (1988) and PhD (1991) degrees in Electrical Engineering are from the University of Wisconsin-Madison. His research activities focus on the study of stability, modeling, simulation, control, optimization, and computational issues in large and small girds and energy systems in the context of competitive energy markets and smart grids. In these areas, he has led or been an integral part of many grants and contracts from government agencies and companies, and has collaborated with industry and university researchers in Canada and abroad, supervising/co-supervising many research fellows and graduate students. He has authored/co-authored a large number of journal and conference papers, as well as various technical reports, book chapters, disclosures and patents, and has been invited to make multiple keynote speeches, seminars, and presentations at many institutions and conferences world-wide. He is an IEEE Fellow, as well as a Fellow of the Royal Society of Canada, where he is currently the Director of the Applied Science and Engineering Division of the Academy of Science, and a Fellow of the Canadian Academy of Engineering. He is also the recipient of the 2017 IEEE Power & Energy Society (PES) Outstanding Power Engineering Educator Award, the 2016 IEEE Canada Electric Power Medal, and of various IEEE PES Technical Council and Committee awards and recognitions, holding leadership positions in several IEEE-PES Technical Committees, Working Groups and Task Forces.

Kankar Bhattacharya (M'95,SM'01,F'17) received the Ph.D. degree in electrical engineering from the Indian Institute of Technology, New Delhi, India, in 1993. He was with the Faculty of Indira Gandhi Institute of Development Research, Mumbai, India, from 1993 to 1998, and with the Department of Electric Power Engineering, Chalmers University of Technology, Gothenburg, Sweden, from 1998 to 2002. In 2003, he joined the Electrical and Computer Engineering Department, University of Waterloo, Waterloo, ON, Canada, where he is currently a full Professor. His current research interests include power system economics and operational aspects. He is a Registered Professional Engineer in the province of Ontario.